Cross sections for electron capture in H^+-Li($2p\sigma,\pi^{\pm}$) collisions

L. Liu,[1,2] C. H. Liu,[2,3] J. G. Wang,[2] and R. K. Janev[4,5]

[1]*College of Physical Sciences, Graduate University of the Chinese Academy of Sciences, P. O. Box 4588, P. R. China*

[2]*Key Laboratory of Computational Physics, Institute of Applied Physics and Computational Mathematics, P. O. Box 8009-26, Beijing 100088, P. R. China*

[3]*Institute of Modern Physics of the Chinese Academy of Sciences, Lanzhou 730000, P. R. China*

[4]*Macedonian Academy of Sciences and Arts, P. O. Box 428, 1000 Skopje, Macedonia*

[5]*Institute of Energy and Climate Research-Plasma Physics, Forschungszentrum Jülich GmbH, Association EURATOM-FZJ, Trilateral Euregio Cluster, D-52425 Jülich, Germany*

(Received 30 June 2011; published 15 September 2011)

State-selective and total single-electron-capture cross sections in collisions of H^+ with the excited Li*(2p) atom have been investigated by using the full quantum-mechanical molecular orbital close-coupling (QMOCC) method in the energy range 0.001–3 keV/u and by the two-center atomic orbital close-coupling (TC-AOCC) method in the energy range 0.1–100 keV/u. The present results are also compared with data from other sources when available. It is found that the total and partial electron-capture cross sections are sensitive to the initial p-state charge cloud alignment, particularly in the low-energy region.

DOI: 10.1103/PhysRevA.84.032710 PACS number(s): 34.70.+e, 34.50.Fa

I. INTRODUCTION

Charge-transfer processes in atom-multicharged ion collisions have been subject to extensive theoretical and experimental studies during the past five decades. The important role of these processes in many laboratory and astrophysical plasmas stems from their large cross sections and pronounced final-state selectivity [1]. Most of these studies have concentrated on target atoms in spherically symmetric ground states. Presently it is possible to use tunable dye lasers as a tool for the preparation of target atoms in specific excited states with a specific alignment (i.e., with a controlled spatial anisotropy of the electronic charge cloud distribution [2]). As compared to the spherically symmetric ground-state target atoms, orbital-alignment-dependent collisions can provide additional insight in the collision dynamics [3]. The study of electronic orientation and charge cloud alignment in heavy particle collisions has become recently an active research field which has attracted both experimental and theoretical attention.

In the present work we shall study the electron-capture process in H^+-Li($2p\sigma,\pi^{\pm}$) collisions by using the full quantum-mechanical molecular-orbital close-coupling (QMOCC) and the two-center atomic orbital close-coupling (TC-AOCC) methods in the energy ranges 0.001–3 keV/u and 0.1–100 keV/u, respectively. To the best of our knowledge, there are no experimental results involving Li*(2p) initial excited states colliding with protons. On the theoretical side, this process has been subject to many theoretical studies using various methods to describe its dynamics. Large-scale semiclassical close-coupling (CC) cross-section calculations have been performed by using the atomic orbital close-coupling (AOCC) [4,5] and molecular orbital close-coupling (MOCC) [6–9] methods, as well as the numerical solution of the time-dependent Schrödinger equation (TDSE) [10].

The main motivation of the present study is to extend the low-energy collision regime for the considered collision system down to 1 eV/u by using the quantal version of the MOCC method (QMOCC) and to test the accuracy of the results of previous calculations in the medium-to high-energy region by using a significantly larger expansion basis in the AOCC method than previously. In applying the AOCC method we have used a model potential for the target that describes accurately the target states.

The paper is organized as follows. In the next section we briefly outline the theoretical methods used in the present study. In Sec. III we present the *ab initio* molecular structure data calculated by the multireference single- and double-excitation configuration interaction (MRD-CI) method [11,12]. In Sec. IV we show the calculated results for the total and state-selective electron-capture cross sections from the $2p\sigma$ and $2p\pi^{\pm}$ excited states of Li in the considered energy range (10^{-3}–100 keV/u). In Sec. V we give our conclusions.

Atomic units will be used throughout, unless explicitly indicated otherwise.

II. THEORECTICAL METHODS

A. TC-AOCC method

The application of the TC-AOCC method to an ion-atom collision system requires the determination of single-center electronic states over which the total scattering wave function is expanded and used in the TDSE to generate the coupled equations for the state amplitudes. For determining the bound electronic states on the target and projectile ions, we have used the variational method with an even-tempered basis [13,14]

$$\begin{aligned}\chi_{klm}(\vec{r}) &= N_l(\xi_k) r^l e^{-\xi_k r} Y_{lm}(\vec{r}),\\ \xi_k &= \alpha\beta^k, \quad k = 1,2,\ldots,N,\end{aligned} \tag{1}$$

where $N_l(\xi_k)$ is a normalization constant, $Y_{lm}(r)$ are the spherical harmonics, and α and β are variational parameters, determined by minimization of the energy. The atomic states $\phi_{nlm}(\vec{r})$ are then obtained as the linear combination

$$\phi_{nlm}(\vec{r}) = \sum_k c_{nk}\chi_{klm}(\vec{r}), \tag{2}$$

where the coefficients c_{nk} are determined by the diagonalization of a single-center Hamiltonian. This diagonalization yields the energies E_{nl} of bound states. In the collision energy range considered in the present paper (0.1–100 keV/u), the straight-line approximation for the relative nuclear motion $R(t) = \vec{b} + \vec{v}t$ (b is the impact parameter and v is the collision velocity) can be safely adopted due to the small binding energy of the $2p$ electron of Li. The TC-AOCC equations are obtained by expanding the total electron wave function Ψ in terms of bound atomic orbitals, multiplied by plane-wave electron translational factors (ETFs) [15]

$$\Psi(\vec{r},t) = \sum_i a_i(t)\phi_i^A(\vec{r},t) + \sum_j b_j(t)\phi_j^B(\vec{r},t), \tag{3}$$

and its insertion in the TDSE $(H - i\frac{\partial}{\partial t})\Psi = 0$. Here, $H = -\frac{1}{2}\nabla_r^2 + V_A(r_A) + V_B(r_B)$, and $V_{A,B}(r_{A,B})$ are the electron interactions with the projectile (H^+) and target (Li^+) cores, respectively. For the second case we have adopted the model potential

$$V_{\rm Li}(r) = -\frac{1}{r} - \frac{1}{r}(2 + 3.310r)e^{-3.310r}, \tag{4}$$

taken from Ref. [16]. The model potential (4) has been obtained by using the unrestricted Ritz variational method.

The resulting first-order coupled equations for the amplitudes $a_i(t)$ and $b_j(t)$ are

$$i(\dot{A} + S\dot{B}) = HA + KB, \tag{5a}$$

$$i(\dot{B} + S^\dagger\dot{A}) = \bar{K}A + \bar{H}B, \tag{5b}$$

where A and B are the vectors of amplitudes a_i ($i = 1, 2, \ldots, N_A$) and b_j ($j = 1, 2, \ldots, N_B$), respectively. S is the overlap matrix ($S^\dagger$ is its transposed form), H and $\bar{H}$ are direct coupling matrices, and K and $\bar{K}$ are the electron exchange matrices. The system of equations (5) is to be solved under the initial conditions

$$a_i(-\infty) = \delta_{1i}, \quad b_j(-\infty) = 0. \tag{6}$$

After solving the system of coupled equations (5a), the cross section for $1 \to j$ electron-capture transition is calculated as

$$\sigma_{cx,j} = 2\pi \int_0^\infty |b_j(+\infty)|^2 b db. \tag{7}$$

The sum of $\sigma_{cx,j}$ over j gives the corresponding total electron-capture cross section.

B. QMOCC method

A detailed description of the QMOCC method is given in Refs. [17,18], and here only a brief account is presented. The QMOCC method involves the solution of a coupled set of second-order differential equations using the log-derivative method of Johnson [19]. In the adiabatic representation, transitions between channels are driven by radial and rotational (A^r and A^θ) couplings of the vector potential $\vec{A}(\vec{R})$, where $\vec{R}$ is the internuclear distance vector. The allowance for the translation effects was made by transforming the radial and rotational coupling matrix elements between the states ψ_K and ψ_L into [20]

$$\begin{aligned} &\langle\psi_K|\partial/\partial R - (\varepsilon_K - \varepsilon_L)z^2/2R|\psi_L\rangle, \\ &\langle\psi_K|iL_y + (\varepsilon_K - \varepsilon_L)zx|\psi_L\rangle, \end{aligned} \tag{8}$$

where ε_K and ε_L are the electronic energies of states ψ_K and ψ_L, and z^2 and zx are the components of the quadrupole moment tensor. The modification is similar in form to that resulting from the application of the common translation factor (ETF) method [21].

Since the adiabatic description contains first- and second-order derivatives, it is numerically convenient to make a unitary transformation [18,22] to a diabatic representation. With the diabatic potentials and couplings, the coupled set of second-order differential equations is solved and matched to the plane-wave boundary conditions at a large internuclear distance $R_{\rm max}$ to obtain the K matrix. Then the scattering matrix S is given by

$$S_J = [I + iK_J]^{-1}[I - iK_J], \tag{9}$$

where I is the identity matrix and J is the total angular momentum quantum number. Finally, the charge-transfer cross section from the channel α to a channel β is expressed in terms of scattering matrix elements

$$\sigma_{\alpha\to\beta} = \frac{\pi}{k_\alpha^2}\sum_J (2J+1)\left|\delta_{\alpha\beta} - S^J_{\alpha\beta}\right|^2, \tag{10}$$

where k_α denotes the initial momentum of the center-of-mass motion.

III. MOLECULAR STRUCTURE CALCULATIONS

An *ab initio* configuration interaction (CI) calculation has been carried out for the potential energy curves of the lower eleven $^2\Sigma$, six $^2\Pi$ and two $^2\Delta$ electronic states of the LiH^+ molecule by using the MRD-CI package [11,12]. In the calculations of hydrogen, the correlation-consistent, polarization valence, quadruple-ζ-(cc-pVQZ)-type basis set [23] with a diffuse $(2s3p3d)$ set was used. The cc-PVQZ-type basis set [23] with a diffuse $(1s1p1d)$ basis was employed also for the Li atom, but the f- and g-type orbitals were discarded. The final contracted basis set for the hydrogen atom was (8s, 6p, 5d)/[6s, 6p, 5d] and that for the Li atom was (13s, 7p, 4d)/ [6s, 5p, 4d]. A threshold of 10^{-8} hartree was used to select the configurations of LiH^+ at the internuclear distances between 0.2 and 50 a.u. The obtained electronic wave functions were then used to calculate the radial and rotational couplings by employing finite-element differentiation and analytical approaches, respectively (see Ref. [24]).

The potential energy curves of molecular states up to H ($n = 3$)/Li($n = 3$) of the LiH^+ ion, calculated in the present work, are shown in Fig. 1 for the internuclear distances $R =$ 0–50 a.u. Apparent on this figure are the sharp, avoided crossings between certain potential curves having the same symmetry (e.g., between $4\,^2\Sigma$ and $5\,^2\Sigma$ at $R \approx 11a_0$, $3\,^2\Pi$ and $4\,^2\Pi$ at $R \approx 7a_0$, $8\,^2\Sigma$, and $9\,^2\Sigma$ at $R \approx 12a_0$).

In Fig. 2 we show the radial coupling matrix elements between the Σ [Fig. 2(a)] and between the Π [Fig. 2(b)] states of the system with the ETF effects included. The sharply peaked radial couplings in these figures correspond to the states

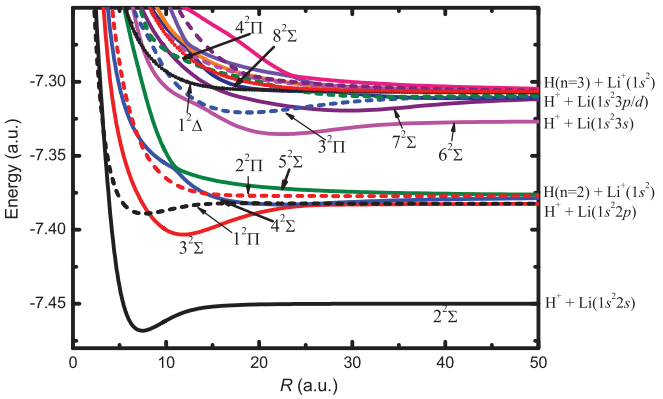

FIG. 1. (Color online) Potential energy curves of the LiH^+ molecular ion. Solid lines: Σ states; dashed lines: Π states; dotted lines: Δ states.

exerting an avoided crossing (some of them mentioned above, cf., Fig. 1) where they are strongly coupled (Landau-Zener coupling). The broad but strong radial couplings between the molecular states converging to the asymptotic configurations Li(2p) and H(n = 2) observed at $R \approx 26a_0$ for the 3 $^2\Sigma$-4 $^2\Sigma$ states [cf. Fig. 2(a)] and at $R \approx 15a_0$ for the 1 $^2\Pi$-2 $^2\Pi$ states [cf. Fig. 2(b)] are due to the change of the character of the electron wave function from an atomic (localized) to a molecular (delocalized) one (Demkov coupling). Such types of couplings are also present between the molecular states that converge to the $Li^+ + H(n = 3)$ and $H^+ + Li(n = 3)$ asymptotic states.

In Fig. 3 we show the most important rotational couplings in the LiH^+ system between the Σ and Π states converging to the n = 2 [Fig. 3(a)] and n = 3 [Fig. 3(b)] states of H or Li. In Fig. 3(a) we should note the particularly large values of the rotational coupling between the states that converge asymptotically to the configurations $H^+ + Li(2p\sigma,\pi)$ or $Li^+ + H(2p\sigma,\pi)$, and extend to large internuclear distances. Similar characteristics exhibit the rotational couplings that couple the states asymptotically converging to the $H^+ + Li(3p\sigma,\pi/3d\sigma,\pi,\delta)$ or $Li^+ + H(3p\sigma,\pi/3d\sigma,\pi,\delta)$ configurations. These couplings are not shown in the figures because the corresponding states are energetically far away from the initial state Li(2p); their couplings contribute little to the total electron capture, but can significantly affect the distribution between these states after the collision.

We note that the π and δ molecular orbitals have a defined symmetry with respect to the collision plane: symmetric (π^+, δ^+), which lie on the collision plane, and antisymmetric (π^-, δ^-), which are perpendicular to the collision plane. These two types of states are not mutually coupled, which results in the decoupling of QMOCC equations with respect to this symmetry. It is also important to note that the molecular states describing the capture channels at large internuclear distances go over to the hydrogen Stark states (produced by the field of the Li^+ ion). To obtain the capture results in the angular momentum representation of atomic states, the corresponding Stark states have to be projected onto angular momentum states. Thus, the $4^2\Sigma(H(2\phi_1))$ and $5^2\Sigma(H(2\phi_2))$ molecular states at large internuclear distances correspond to the Stark states built as linear combinations of atomic angular momentum states

$$|2\phi_{1,2}\rangle = \frac{1}{\sqrt{2}}[|2s\rangle \pm |2p\sigma\rangle]. \tag{11}$$

In the $n = 3$ σ subspace, the molecular Σ states at large internuclear distances correspond to the Stark states representing the linear combinations of atomic states

$$\begin{aligned} |3\varphi_1\rangle &= \frac{1}{\sqrt{3}}|3s\rangle + \frac{1}{\sqrt{2}}|3p\sigma\rangle + \frac{1}{\sqrt{6}}|3d\sigma\rangle, \\ |3\varphi_2\rangle &= \frac{1}{\sqrt{3}}|3s\rangle - \sqrt{\frac{2}{3}}|3d\sigma\rangle, \\ |3\varphi_3\rangle &= \frac{1}{\sqrt{6}}\left[\frac{1}{\sqrt{3}}|3s\rangle - \frac{1}{\sqrt{2}}|3p\sigma\rangle\frac{1}{\sqrt{6}}|3d\sigma\rangle\right]. \end{aligned} \tag{12}$$

The correspondence of molecular $p\pi^\pm$ and $d\delta^\pm$ states with corresponding atomic states is straightforward.

IV. RESULTS AND DISCUSSIONS

The state-selective and total single-electron-capture cross sections for H^+-Li(2p) collisions have been calculated by the QMOCC method and AOCC method in the energy range 0.001–3 and 0.1–100 keV/u, respectively. In the present AOCC calculations we have included in the basis all the states with $n \leqslant 6$ centered on H, and the states with $n = 2, 3$ centered

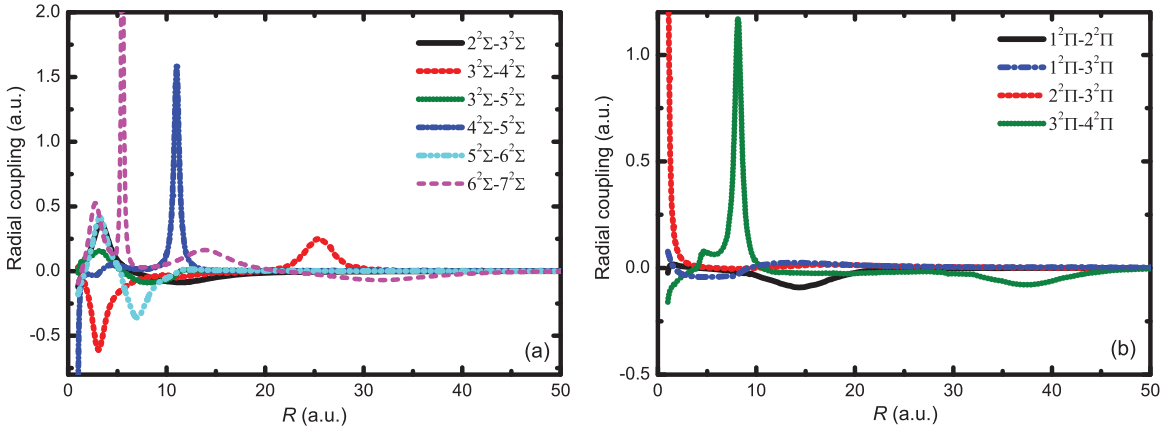

FIG. 2. (Color online) Radial coupling matrix elements between (a) the Σ and (b) between the Π states of LiH^+.

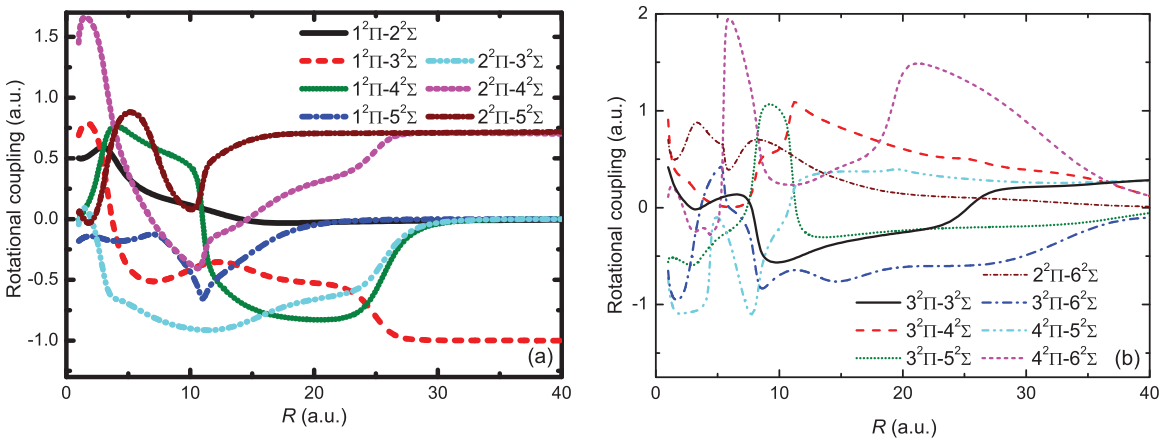

FIG. 3. (Color online) Rotational coupling matrix elements between the Σ and Π states of LiH^+ ion asymptotically converging to (a) $n = 2$ and (b) $n = 3$ states of Li or H.

on Li, in total 104 states. In the QMOCC calculations, all Σ, Π, and Δ molecular orbitals (MO) were used correlating asymptotically to the $n = 2$, 3 states of Li and H, in total 26 molecular states.

A. Capture to $n = 2$ states of H

In Fig. 4 we present the results of the present QMOCC and AOCC calculations for electron capture from the initial Li($2p\sigma$) state to the $2s$ and $2p$ states of H. The present results are compared with the results for $E = 5$, 10, 15 keV/u of Ref. [10], obtained by the TDSE method, and with the semiclassical MOCC results of Ref. [9] obtained with a 26 MO basis (the same as the one used in the present QMOCC calculations) but using a model potential for the electron-core interaction in Li($2p$) of the same form as Eq. (4). In the calculations of other authors (Refs. [4–8]) such state-selective cross sections are not reported. It is to be noted in this figure that the present QMOCC and AOCC results for capture to the $2s$ and $2p$ state of H are in a fairly good mutual agreement in the overlapping energy range. The $2p$ capture results of Ref. [9] agree well with

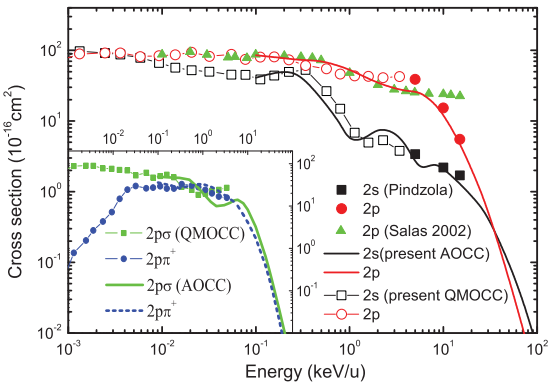

FIG. 4. (Color online) State-selective cross sections for electron capture to $2l$ states of H atom from the Li($2p\sigma$) initial state. Open symbols and solid lines present QMOCC and AOCC results, respectively; solid triangles: MOCC results of Ref. [9]; solid circles and solid squares: TDSE results of Ref. [10]. Inset: Solid symbols: present QMOCC results; solid lines present AOCC results.

our AOCC and QMOCC results in the energy range of 0.01–6 keV/u. The results of the authors of Ref. [10] also show a good agreement with our AOCC results. It is interesting to note that both the QMOCC and AOCC $2s$ and $2p$ capture cross sections show an oscillatory behavior for energies in the range 0.1–10 keV/u. This structure is generated by the existence of two consecutive strong coupling regions, the Demkov $3\,^2\Sigma$-$4\,^2\Sigma$ coupling at $R \approx 26a_0$ and the Landau-Zener $4\,^2\Sigma$-$5\,^2\Sigma$ coupling at $R \approx 11a_0$, where the probability flux undergoes branching during both the incoming and outgoing stages of the collision.

The QMOCC calculations have shown that the cross sections $\sigma(2p\sigma)$ and $\sigma(2p\pi^+)$, contributing to the $\sigma(2p)$ cross section shown in Fig. 4, have comparable values in the energy region above ∼0.3 keV/u, in the energy range 0.03–0.3 keV/u the $\sigma(2p\sigma)$ cross section is about two times larger than $\sigma(2p\pi^+)$ (which in the entire 0.03–1 keV/u range remains quasi-constant), while for $E \leqslant 0.03$ keV/u, the cross section $\sigma(2p\pi^+)$ exponentially (adiabatically) decreases with decreasing energy (see the inset in Fig. 4). This energy behavior of the $\sigma(2p\pi^+)$ cross section results from the fact that for the initial Li($2p\sigma$) state, the H($2p\pi^+$) capture state is populated mainly [see Figs. 1 and 3(a)] by the $3\,^2\Sigma$-$2\,^2\Pi$, $4\,^2\Sigma$-$2\,^2\Pi$, and $3\,^2\Sigma$-$1\,^2\Pi$ rotational couplings at relatively small internuclear distances (the $1\,^2\Pi$ and $2\,^2\Pi$ states being Demkov-mixed at $R \approx 25a_0$) which are unattainable at very low energies. The QMOCC calculations have also shown that the $\sigma(2s)$ and $\sigma(2p\sigma)$ cross sections are very close to each other in the entire energy region below ∼1 keV/u. The proximity of these two cross sections, especially in the region below ∼0.01 keV/u (as observed also in Fig. 4), results from the quasi-degeneracy of $4\,^2\Sigma$ and $5\,^2\Sigma$ molecular states at large internuclear distances [cf., Fig. 1 and Eq. (11)].

The capture cross sections to $2s$ and $2p$ states of H from the initial Li($2p\pi^+$) state of the present QMOCC and AOCC calculations are shown in Fig. 5 and compared with the results of the authors of Ref. [9]. In Ref. [10] only the half-sum of the populations of these states from Li($2p\pi^+$) and Li($2p\pi^-$) initial states is given, so that a direct comparison of the two sets of results cannot be made. The present QMOCC $2p$ results show good agreement with the AOCC results, but are somewhat larger than the MOCC results of the authors of

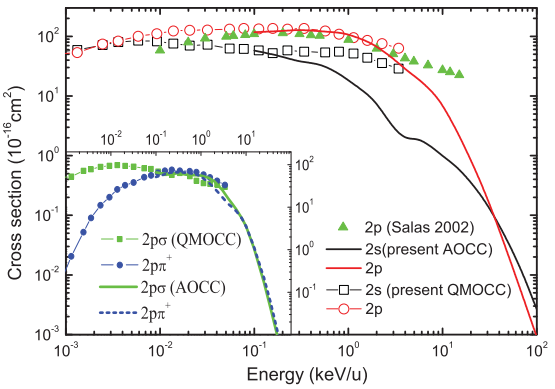

FIG. 5. (Color online) State-selective cross sections for electron capture to $2l$ states of H from the Li$(2p\pi^+)$ initial state. Open symbols and solid lines present QMOCC and AOCC results, respectively; solid triangles: MOCC results of Ref. [9]. Inset: Solid symbols: present QMOCC results; solid lines: present AOCC results.

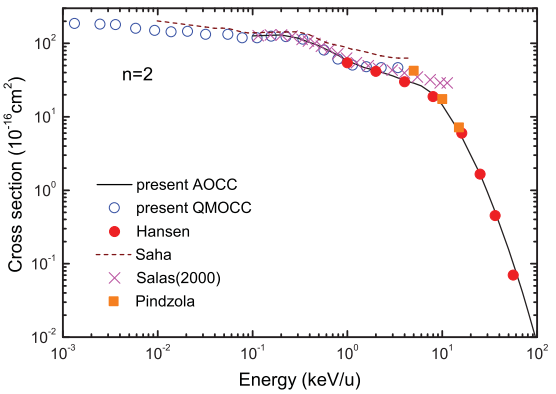

FIG. 6. (Color online) Cross sections for electron capture to $n = 2$ shell of H from Li$(2p\sigma)$ state. (—) present AOCC results; (○) present QMOCC results; (●) AOCC results of Hansen *et al.* [4]; (—·—) results of Saha *et al.* [8]; (×) results of Salas *et al.* [6]; (■) results of Pindzola *et al.* [10].

Ref. [9] in the energy region below $E = 0.2$ keV/u. Since the MO basis in Ref. [9] was the same as in the present work, the difference between the two results in the $E < 0.2$ keV/u region can be ascribed to the use of a model potential in Ref. [9] for the e-Li$^+$ interaction. The figure also shows that the present QMOCC and AOCC results disagree considerably for energies larger than 0.2 keV/u. The reason for this disagreement could be that for this capture channel both QMOCC and AOCC methods enter the energy region of their inapplicability. We note that the MOCC results of Ref. [9] tend to overestimate the cross section for energies above ~ 3 keV/u, an indication of the inadequacy of the MOCC description of collision dynamics at these energies (despite the large 26 MO basis used).

The collision dynamics in the case of the Li$(2p\pi^+)$ initial state is essentially governed by the Demkov coupling of $1\,^2\Pi$ and $2\,^2\Pi$ states at $R \approx 15a_0$ in the incoming stage of the collision, by the rotational $1\,^2\Pi$-$3\,^2\Sigma$, $2\,^2\Pi$-$3\,^2\Sigma$, and $2\,^2\Pi$-$4\,^2\Sigma$ couplings at small internuclear distances, and by the Landau-Zener $4\,^2\Sigma$-$5\,^2\Sigma$ coupling at $R \approx 11a_0$ and Demkov $3\,^2\Sigma$-$4\,^2\Sigma$ and $1\,^2\Pi$-$2\,^2\Pi$ couplings at $R \approx 26a_0$ and $R \approx 15a_0$, respectively, in the outgoing stage of the collision [cf., Figs. 1 and 3(a)]. The QMOCC calculations have shown that the $\sigma(2s)$ and $\sigma(2p\sigma)$ capture cross sections are close to each other in the entire 0.001–3 keV/u energy range and that the $\sigma(2p\pi^+)$ cross section is larger than $\sigma(2s)$ and $\sigma(2p\sigma)$ for $E \geqslant 0.15$ keV/u, but becomes smaller for $E \leqslant 0.06$ keV/u and then rapidly (adiabatically) decreases with decreasing energy (see the inset in Fig. 5).

The charge transfer cross sections for the transition Li$(2p\sigma)\rightarrow$H$(n = 2)$, calculated by QMOCC and AOCC methods, are presented in Fig. 6. In the same figure we also show the cross-section results obtained previously by using the AOCC [4], semi-classical MOCC [6,8], and TDSE [10] methods for comparison. There are no experimental data available for this process. The present QMOCC and AOCC results are in good mutual agreement in the overlapping energy range, as well as with the semiclassical MOCC results of Salas [6]. We mention again that in Ref. [6] the interaction of the valence electron in Li with the ion core was represented by a model potential of the same form as Eq. (4) and 26 MO (with a common electron translational factor (ETF) taken from Ref. [25]) were included in the MOCC dynamics. We further note that the semiclassical MOCC results of Ref. [7] (with eight MOs; not shown in the figure) are significantly larger than those of Ref. [6] for energies above 1 keV/u. The MOCC results of Saha *et al.* [8] obtained with a six MO basis (and an l-dependent pseudopotential for the e-Li$^+$ interaction) are somewhat larger than all other presented theoretical results, a consequence of the smaller basis. The previous AOCC [4] and TDSE [10] results agree well with the present AOCC result for energies above 1 and 10 keV/u, respectively. We mention that in Ref. [4] a model potential practically identical with Eq. (4) was used (the values 3.310 being replaced by 3.3117) and the $n = 2$,3 states on Li and $n = 1$, 2, 3 states on H (altogether 27 states) were included in the expansion basis. The good agreement of the present AOCC results with those of Ref. [4] up to about 50 keV/u is, therefore, not surprising. The slight disagreement between the two sets of AOCC data at energies above 50 keV/u is likely to originate from the difference in the size of the AO bases employed.

The cross sections for electron capture to H$(n = 2)$ from the initial Li$(2p\pi^+)$ state, obtained from the present QMOCC

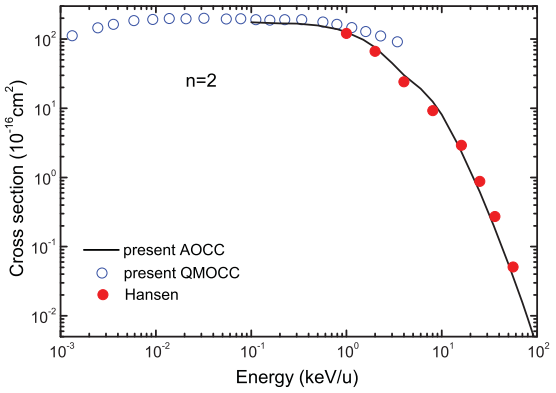

FIG. 7. (Color online) Cross sections for electron capture to $n = 2$ shell of H from the initial Li$(2p\pi^+)$ state. Open circles and solid line are the present QMOCC and AOCC results, respectively; solid circles are the AOCC results of Ref. [4].

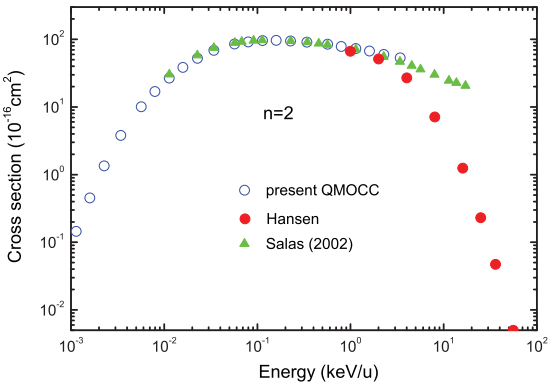

FIG. 8. (Color online) Cross sections for electron capture to $n = 2$ shell of H from Li ($2p\pi^-$) initial state. Open circles: present QMOCC results; closed triangles: MOCC results of Ref. [9]; solid circles: AOCC results of Ref. [4].

and AOCC calculations, are shown in Fig. 7, and are compared with the AOCC results from Ref. [4]. In the overlapping energy range 0.1–1 keV/u, our QMOCC and AOCC results are in good mutual agreement. However, for $E > 1$ keV/u, the QMOCC results lie significantly above the present AOCC results, most probably due to the inadequate description of the electron momentum transfer effects in the QMOCC method in this energy region. In the energy region above 1 keV/u, the present AOCC results are in good agreement with the AOCC results of Hansen *et al.* [4]. In Refs. [5,6,8,10], only the half-sum of the populations of these states from Li($2p\pi^+$) and Li($2p\pi^-$) initial states is given.

In Fig. 8 we show the results of present QMOCC cross-section results for electron capture to the $n = 2$ shell of H from the initial Li($2p\pi^-$) state in the energy range 0.001–3 keV/u. The AOCC results of Hansen *et al.* [4] and the semiclassical MOCC results of Salas [9] for capture to the $n = 2$ shell are also shown in this figure as well. Our QMOCC results agree very well with the semiclassical MOCC results of Ref. [9], and are larger than the AOCC results of Ref. [4] for $E > 2$ keV/u. As mentioned above, the MOCC results may overestimate the cross section for $E > 2$ keV/u due to the inadequate description of electron momentum transfer effects. However, the smooth connection of the MOCC and AOCC results for capture to the $n = 2$ shell at $E \sim 1$ keV/u provides a reliable representation of the $n = 2$ cross section in the energy range 1–50 keV/u.

The small magnitude of $n = 2$ capture cross section from the initial Li($2p\pi^-$) state in the low-energy region is a consequence of the fact that only the relatively weak Demkov $1\,^2\Pi$-$2\,^2\Pi$ radial coupling at $R \sim 15a_0$ [cf., Fig. 2(b)] is responsible for the electron capture in this channel. Accordingly, after attaining its broad maximum in the region of 0.1–0.3 keV/u, the cross section adiabatically decreases with decreasing energy.

The large difference in the energy dependence of $n = 2$ capture cross sections from the Li($2p\sigma$, $\pi^\pm$) initial states in the low-energy region (as opposed to their uniform energy behavior for $E > 10$ keV/u), observed in Figs. 6 through 8, reflects the differences in the multitude of reaction paths (and the involved couplings along them) that populate the $n = 2$ shell.

B. Capture to $n = 3$ states of H

The electron capture dynamics in the population of $n = 3$ group of hydrogen atom states from the Li($2p\sigma$,$\pi^\pm$) initial states is initiated (in the molecular picture) by the couplings of $n = 2$ states with $n = 3$ states in the approaching stage of the collision. As Figs. 2 and 3 show, the only strong couplings between these two groups of states are the radial coupling between $5\,^2\Sigma$ and $6\,^2\Sigma$ states at $R \approx 7a_0$ and the $3\,^2\Sigma$-$3\,^2\Pi$, $4\,^2\Sigma$-$3\,^2\Pi$, $5\,^2\Sigma$-$3\,^2\Pi$, $5\,^2\Sigma$-$4\,^2\Pi$, and $2\,^2\Pi$ -$6\,^2\Sigma$ rotational couplings. In the receding stage of the collision there is a multitude of radial couplings between the $n = 3$ group of states having the same symmetry, the most important of them being the Landau-Zener couplings between the states $6\,^2\Sigma$ and $7\,^2\Sigma$ at $R \approx 5.5a_0$, $8\,^2\Sigma$ and $9\,^2\Sigma$ at $R \approx 13a_0$, $3\,^2\Pi$ and $4\,^2\Pi$ at $R \approx 8a_0$, and the Demkov coupling of $7\,^2\Sigma$ and $8\,^2\Sigma$ states at $R \approx 45a_0$ (see Figs 1–3). We shall not analyze the reaction paths leading to the population of a given $3lm^{(\pm)}$ from a given Li($2p\sigma$,$\pi^\pm$) initial state, but rather present only the $3l$ capture cross sections.

In Fig. 9 we show the present QMOCC and AOCC cross-section results for capture to the $3l$ states of H from the initial Li($2p\sigma$) state. The TDSE results of Pindzola *et al.* [10] for 5, 10, and 15 keV/u are also shown in the figure. The present AOCC results are in good agreement with the results of the authors of Ref. [10], except for the energy of 10 keV/u in the $3s$ and $3p$ capture cross sections where the results of the authors of Ref. [10] are somewhat larger than ours. For the $3d$ capture cross section, the present AOCC and QMOCC result agree well in the overlapping energy range (except at 2 and 3 keV/u, where the QMOCC overestimates the cross section). However, the AOCC and QMOCC $3s$ and $3p$ capture cross sections significantly disagree in the overlapping energy range: above ~1 keV/u the QMOCC cross sections are smaller than the AOCC ones, while for E below ~0.2 keV/u they are higher. The disagreement for E above ~1 keV/u could be due to the insufficient size of the molecular basis used in QMOCC calculations, while that for E below ~0.2 keV/u is due to the invalidity of the AOCC method at these energies when describing the weak channels.

Figure 9 shows that both the QMOCC and AOCC $3s$ and $3p$ capture cross sections exhibit oscillatory structures

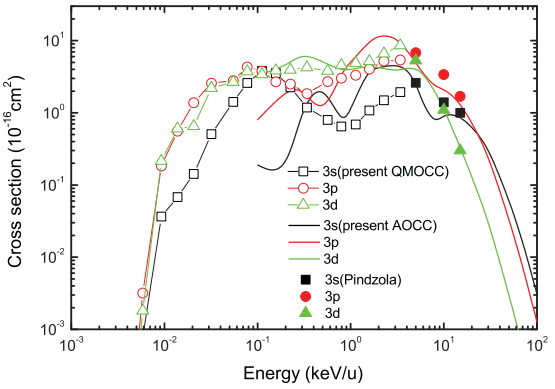

FIG. 9. (Color online) State-selective cross sections for electron capture to $3l$ states of H atom from the Li($2p\sigma$) initial state. Open symbols and solid lines are the present QMOCC and AOCC results, respectively; solid symbols are the TDSE results of Ref. [10].

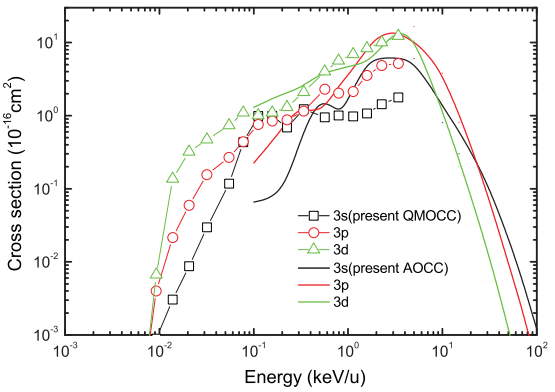

FIG. 10. (Color online) State-selective cross sections for electron capture to $3l$ channels of H atom from Li ($2p\pi^+$) initial state.

in the energy range 0.1–10 keV/u. This can be related to the complexity of couplings within the H($n = 3$) and Li ($n = 3$) groups of states. It should also be remarked that with respect to the capture to $2l$ states from the initial Li($2p\sigma$) state, the magnitude of $3l$ capture cross sections is an order of magnitude smaller than those for capture to the $2l$ states. This is to be expected since the initial Li($2p\sigma$) state is energetically much closer to the H($2l$) group of states at large internuclear distances than to the H($3l$) group of states and since the radial couplings within the $n = 2$ group of states are much stronger than those between the $n = 2$ and $n = 3$ groups of states. Another important difference between the $\sigma(3l)$ and $\sigma(2l)$ cross sections for capture from the initial Li($2p\sigma$) state is that the $\sigma(2l)$ cross sections continue to be large down to 10^{-3} keV/u (and even below this energy; see Fig. 4), while the $\sigma(3l)$ cross sections all exhibit a strong (adiabatic) decrease below $\sim$0.03 keV/u. This is again a consequence of the difference in the strength of the couplings within the $n = 2$ group of states and the couplings between the $n = 2$ and $n = 3$ groups of states. These arguments remain obviously valid also when the initial state is Li($2p\pi^{\pm}$), as we shall see in the next figures.

The results of present QMOCC and AOCC calculations for capture to H($3l$) states from the initial Li($2p\pi^+$) state are shown in Fig. 10. As in the case of the Li($2p\sigma$) initial state, the QMOCC cross sections for capture to $3s$ and $3p$ states are higher than the AOCC results for $E < 0.2$ keV/u, but lower than the AOCC ones for $E > 1$ keV/u. These discrepancies have the same origin as in the previous case. Compared to the results for the Li($2p\sigma$) initial state, the cross sections in the present case, however, show much less pronounced oscillatory behavior in the 0.1–1 keV/u energy range.

The present QMOCC and AOCC cross sections for electron capture to H($n = 3$) shell from the initial Li($2p\sigma$) state are shown in Fig. 11, together with the AOCC results of Hansen *et al.* [4], MOCC results of Salas *et al.* [6], and TDSE results of Pindzola *et al.* [10]. In the energy range 0.2–3 keV/u, the QMOCC results are somewhat lower than the AOCC results, while for energies below 0.2 keV/u the QMOCC results become higher than the AOCC results. The present AOCC results are in good agreement with the AOCC data of Hansen *et al.* [4] and TDSE results of Pindzola *et al.* [10] for energies above 4 keV/u. The MOCC results of Salas [6] agree

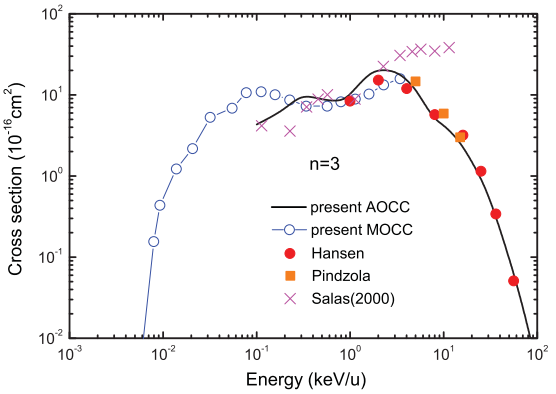

FIG. 11. (Color online) Cross sections for electron capture to $n = 3$ shell of H from Li($2p\sigma$) initial state. Open circles and solid line: present QMOCC and AOCC results, respectively; solid circles: AOCC results of Ref. [4]; crosses: MOCC results of Ref. [6]; solid squares: TDSE results of Ref. [10].

with the present results to a certain extent for energies below 2 keV/u, but for $E > 2$ keV/u they are significantly larger than our AOCC results (most probably due to the inadequate description of electron momentum translational effects).

The cross sections for electron capture to the $n = 3$ shell of H from the Li($2p\pi^+$) initial state, obtained by the QMOCC and AOCC methods, are presented in Fig. 12. For comparison, the cross section of AOCC method by Hansen *et al.* [4] is also shown in the figure. The present QMOCC and AOCC results are in good mutual agreement in the overlapping energy range of 0.1–1 keV/u. Above 1 keV/u, the present QMOCC results are slightly lower than the AOCC results. In the energy region 1–100 keV/u, the present AOCC results are in good agreement with the AOCC results by Hansen *et al.* [4].

Figure 13 shows the cross sections for electron capture to H($n = 3$) from the Li($2p\pi^-$) initial state obtained by the QMOCC method. The AOCC results of Hansen *et al.* are also shown for comparison. The figure shows that in the overlapping energy range, the present QMOCC results are lower than the AOCC results of Hansen *et al.*, possibly due to the insufficient expansion basis used in the present calculations. For this process there no other theoretical data

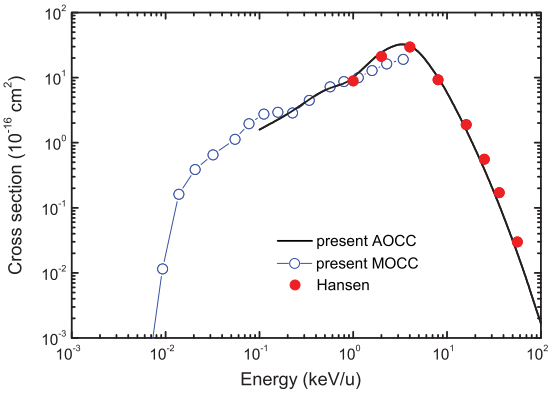

FIG. 12. (Color online) Cross sections for electron capture to $n = 3$ shell of H from the initial Li($2p\pi^+$) state. Open circles and solid line are present QMOCC and AOCC results, respectively; solid circles are the AOCC results of Ref. [4].

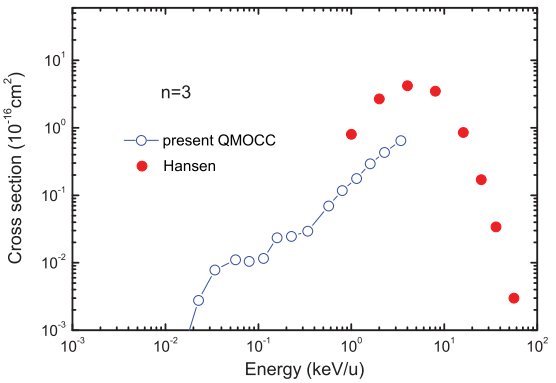

FIG. 13. (Color online) Cross sections for electron capture to $n = 3$ shell of H from the Li($2p\pi^-$) initial state. Open circles: present QMOCC results; closed circles: AOCC results of Ref. [4].

available. The magnitude of the cross section for capture to the $n = 3$ shell of H from the Li($2p\pi^-$) initial state is much smaller than those for capture from the Li($2p\sigma,\pi^+$) initial states, particularly in the low-energy region (see Figs. 11 and 12). The reason is the series of weak couplings (the Demkov $1\,^2\Pi$-$2\,^2\Pi$ coupling at $R \approx 15a_0$ and the Landau-Zener $2\,^2\Pi$-$3\,^2\Pi$ coupling at $R \approx 1.5a_0$) that promote the $p\pi^-$ molecular state into the group of $n = 3$ states and the symmetry constrains on $2p\pi^-$-$np\pi^-$ transitions.

V. CONCLUSION

In the present article we have studied the electron-capture processes in the H^+-Li($2p\sigma,\pi^\pm$) collision system in a broad range of collision energies. The state-selective cross sections for the electron capture have been calculated using the QMOCC method in the energy range 0.001–3 keV/u and the TC-AOCC method in the energy range 0.1–100 keV/u. The *ab initio* molecular structure data, used in the QMOCC calculations, have been calculated by the MRD-CI method. In the AOCC calculations, the interaction of an active electron with the projectile ion has been approximated by a one-particle model potential. The results of the two calculations for the dominant channel capture cross sections agree well in the overlapping energy range. They also agree with the results of other theoretical calculations employing the semiclassical MOCC, AOCC, and TDSE methods.

It has been found that the energy behavior and magnitude of the total and state-selective electron-capture cross sections for the three cases of the H^+-Li($2p\sigma,\pi^\pm$) collision system are similar at high energies. However, a strong alignment dependence on the initial state is obtained for the electron capture to H($n = 2, 3$) states at low energies. The differences in the magnitude and energy behavior of the cross sections for different capture states in this energy region have been discussed on the basis of the molecular picture of collision dynamics. We note that in the case of the H^+-Li($2p\pi^-$) collision system, the partial cross sections for electron capture to H($n = 2, 3$) states are two or three orders of magnitude smaller than the ones in H^+-Li($2p\sigma,\pi^+$) collision cases in the low-energy region. This significant difference in the magnitudes of n-partial cross sections has been understood on the basis of symmetry constrains. When the initial state is Li($2p\pi^-$), the electron can only transit to the H($2p\pi^-$) or H($3p\pi^-$) state. Due to the lack of population via the H($2p\sigma,\pi^+$) states, the cross sections for capture to $n = 2$ and $n = 3$ shells from the Li($2p\pi^-$) initial state will be smaller than in the cases of Li($2p\sigma,\pi^+$) initial states.

ACKNOWLEDGMENTS

This work was supported by the International Atomic Energy Agency (Vienna, Austria) (Research Contract Nos. 15689/R0 with RKJ and 15700/R0 with JGW) and by the National Natural Science Foundation of China (Grant Nos. 10875017, 11025417, 10974021, 11004014, and 10734140).

[1] R. K. Janev, L. P. Presnyakov, and V. P. Shevelko, *Physics of Highly Charged Ions* (Springer, Berlin, 1985).
[2] N. Andersen, J. W. Gallagher, and I. V. Hertel, Phys. Rep. **165**, 1 (1988).
[3] I. V. Hertel and W. Stoll, Adv. At. Mol. Phys. **13**, 113 (1978).
[4] J. P. Hansen, S. E. Nielsen, and J. Schweinzer, J. Phys. B **26**, L471 (1993).
[5] M. F. V. Lundsgaard, S. E. Nielsen, H. Rudolph, and J. P. Hansen, J. Phys. B **31**, 3215 (1998).
[6] P. J. Salas, J. Phys. B **33**, 3201 (2000).
[7] P. J. Salas and P. Wahnón, J. Chem. Soc. Faraday Trans. **89**, 1573 (1993).
[8] B. C. Saha and C. A. Weatherford, J. Mol. Struct. (Theochem.) **388**, 97 (1996).
[9] P. J. Salas, J. Phys. B **35**, 3443 (2002).
[10] M. S. Pindzola, T. Minami, and D. R. Schultz, Phys. Rev. A **68**, 013404 (2003).
[11] R. J. Buenker and R. A. Philips, J. Mol. Struct. Theochem. **123**, 291 (1985).
[12] S. Krebs and R. J. Buenker, J. Chem. Phys. **103**, 5613 (1995).
[13] J. Kuang and C. D. Lin, J. Phys. B **30**, 101 (1997).
[14] C. M. Reeves, J. Chem. Phys. **39**, 1 (1963).
[15] W. Fritsch and C. D. Lin, Phys. Rep. **202**, 1 (1991).
[16] W. L. McMillan, Phys. Rev. A **4**, 69 (1971).
[17] M. Kimura and N. F. Lane, Adv. At. Mol. Opt. Phys. **26**, 79 (1990).
[18] B. Zygelman, D. L. Cooper, M. J. Ford, A. Dalgarno, J. Gerratt, and M. Raimondi, Phys. Rev. A **46**, 3846 (1992).
[19] B. R. Johnson, J. Comput. Phys. **13**, 445 (1973).
[20] M. C. Bacchus-Montabonel and P. Ceyzeriat, Phys. Rev. A **58**, 1162 (1998).
[21] L. F. Errea, L. Mendez, and A. Riera, J. Phys. B. **15**, 101 (1982).
[22] T. G. Heil, S. E. Butler, and A. Dalgarno, Phys. Rev. A **23**, 1100 (1981).
[23] T. H. Dunning Jr., J. Chem. Phys. **90**, 1007 (1989).
[24] G. Hirsch, P. J. Bruna, R. J. Buenker, and S. D. Peyerimhoff, Chem. Phys. **45**, 335 (1980).
[25] S. B. Schneiderman and A. Russek, Phys, Rev. **181**, 311 (1969).